

# Evolution of Microstructure and Mechanical Properties of ATI 718Plus® Superalloy After Graded Solution Treatment



SEBASTIAN LECH, AGNIESZKA M. WUSATOWSKA-SARNEK, KRZYSZTOF WIECZERZAK, and ADAM KRUK

The evolution of microstructure and mechanical properties of ATI 718Plus® superalloy subjected to a graded solution treatment was evaluated. Graded solution treatment was performed on a single bar of 718Plus superalloy for 1 hour within a temperature range of 907 °C to 1095 °C. It resulted in a graded microstructure investigated mainly by light microscopy, scanning-, and transmission electron microscopy. A quantitative analysis of identified phases was performed. Mechanical properties were assessed using the Vickers hardness test and correlated with the microstructural changes. The structure–property relationship between 718Plus superalloy microstructure and mechanical properties was established. The change of the  $\gamma$  phase grain size in the single-phase range did not affect the hardness in a meaningful manner. Significant increases in hardness were observed after the introduction of  $\gamma'$  and  $\eta$  phases. Phase stability limits were determined experimentally and compared with those calculated using the Thermo-Calc software.

<https://doi.org/10.1007/s11661-022-06859-z>  
© The Author(s) 2022

## I. INTRODUCTION

POLYCRYSTALLINE nickel-base superalloys are a group of materials widely used in energy and aeronautics, where their high-temperature microstructural stability is strongly required. A very special alloy in this group is Inconel 718. Although it was introduced as jet engine material in the early 1960s, it is still one of the most used nickel-based superalloys.<sup>[1]</sup> Wide usage of this alloy comes from its excellent heat, corrosion, and creep resistance combined with good workability and moderate price. Mechanical properties of Inconel 718 are predominantly determined by precipitation of disc-shaped  $\gamma''$  phase (D0<sub>22</sub> crystal structure) composed of nickel, niobium, and titanium,<sup>[2–5]</sup> as well as spherical  $\gamma'$  phase (L1<sub>2</sub> crystal structure) containing nickel, aluminum, titanium, and

niobium. However, a critical limitation of Inconel 718 is associated with insufficient microstructural thermal stability above 650 °C due to  $\gamma''$  phase transformation taking place at higher temperatures.<sup>[6]</sup> This drawback, followed by increasing requirements for jet engine operating conditions, has become a driving force to search for materials with improved high-temperature structure stability.<sup>[7]</sup> Those efforts resulted in introducing the ATI 718Plus® (hereafter 718Plus) superalloy in 2004.<sup>[8,9]</sup>

The chemical composition of 718Plus was modified from baseline Inconel 718 by adding alloying elements (Co and Al) promoting precipitation of the  $\gamma'$  phase instead of unstable  $\gamma''$  phase.<sup>[10]</sup> Due to changes in chemical composition in 718Plus superalloy, aging treatment results in precipitation of fine, spherical precipitates of  $\gamma'$  phase. A comparison of Inconel 718 and 718Plus superalloys showed that the size of the strengthening  $\gamma'$  phase in 718Plus is slightly greater than the size of  $\gamma'/\gamma''$  phases in Inconel 718 after standard heat treatments.<sup>[11]</sup> However, further annealing for 500 hours at 760 °C resulted in coarsening of precipitates to 70 nm for 718Plus and 90 nm in Inconel 718, proving more excellent stability of 718Plus at high temperatures. The other effect of the modified chemical composition is the presence of the  $\eta$  phase (D0<sub>24</sub> crystal structure) at the grain boundaries in favor of the  $\delta$  phase (D0<sub>a</sub> crystal structure).<sup>[12–14]</sup> Interestingly, in 718Plus superalloy, grain boundary precipitates were reported by some authors as  $\delta$  phase<sup>[8,10,11]</sup> and others as  $\eta$  phase.<sup>[12–14]</sup> It was found that both sides were

SEBASTIAN LECH and ADAM KRUK are with the International Centre of Electron Microscopy for Materials Science, Faculty of Metals Engineering and Industrial Computer Science, AGH University of Science and Technology, Mickiewicza 30, 30-059 Kraków, Poland. Contact e-mail: slech@agh.edu.pl AGNIESZKA M. WUSATOWSKA-SARNEK is with the Pratt & Whitney, 400 Main Street, M/S 114-40, East Hartford. KRZYSZTOF WIECZERZAK is with the Laboratory for Mechanics of Materials and Nanostructures, Empa, Swiss Federal Laboratories for Materials Testing and Research, Feuerwerkerstrasse 39, 3602 Thun, Switzerland. Manuscript submitted June 27, 2022; accepted October 13, 2022.

Article published online November 8, 2022

correct as, within the microstructure of the 718Plus superalloy, both phases can be found. However, to be precise, in the 718Plus superalloy,  $\eta$  phase is the one predominantly precipitated at the grain boundaries. The detailed studies of Pickering *et al.*,<sup>[12]</sup> Messé *et al.*,<sup>[13]</sup> and present authors<sup>[15]</sup> unambiguously identified those precipitates as  $\eta$  phase. According to Pickering *et al.*,<sup>[12]</sup> the  $\delta$  accounts for less than 1 pct of grain boundary precipitates in the 718Plus superalloy. Thus, referring only to the  $\eta$  phase at grain boundaries seems more accurate. Furthermore, the  $\delta$  phase can be present as planar defects in plates of the  $\eta$  phase.<sup>[15]</sup> The mechanical properties of the 718Plus superalloy are greater than those of Inconel 718 and Waspaloy superalloys.<sup>[10]</sup> After standard heat treatment, 718Plus superalloy demonstrates the highest ultimate tensile strength of almost 1200 MPa and yield strength of about 1000 MPa. Under stress rupture test at 704 °C, lifetime of 718Plus is comparable to Waspaloy; however, it was superior to other superalloys during the creep tests.

Over the years, many properties of 718Plus superalloy have been assessed, like mechanical properties,<sup>[16–18]</sup> oxidation resistance,<sup>[19–21]</sup> and phase stability.<sup>[11,22,23]</sup> Especially mechanical properties can be tailored in a broad range due to numerous available processing techniques<sup>[24,25]</sup> and heat treatment routes.<sup>[26,27]</sup> A selection of proper heat treatment conditions is crucial for nickel-based superalloys to achieve superior high-temperature properties. Despite many possible heat treatment routes for superalloys, solution treatment after thermo-mechanical processing is the first step to achieve desired microstructure. Within this study, a course of solutionizing in 718Plus superalloy was investigated using a graded solution treatment. In the modern world, conventional heat treatment optimization methods are not cost-effective and time consuming. Thus, highly efficient methods in materials science are desired, whether it is a computational<sup>[28,29]</sup> or experimental<sup>[30]</sup> alloy design. The present work focuses on the application of heat treatment with gradient temperature for a 1-hour solution treatment of 718Plus superalloy in a wide range of temperatures. The applied approach resulted in graded microstructure, followed by a gradual change of mechanical properties in terms of microhardness in a single sample. The microstructural changes were later investigated using light- and electron microscopy. Furthermore, it was possible to establish phase stability limits and compared them to the ones calculated using thermodynamic simulations.

Obtained results may be used as guidelines for solution treatment of investigated superalloy. Later, graded heat treatment method could be combined with aging treatment. Overall, present results demonstrate a cost-effective method to investigate phase stability in alloys with high precision supported by structural and mechanical data.

## II. EXPERIMENTAL PROCEDURE

### A. Material

The material used in this study was a commercial 718Plus superalloy (ATI) with a nominal chemical composition of Ni–18Cr–9.7Fe–9.2Co–5.5Nb–2.7Mo–

1W–0.75Ti–1.5Al–0.02C (wt pct). The detailed chemical composition is industrially confidential, although the latter thermodynamic simulations were in good agreement for detailed and nominal ones. It was produced as a commercial scale component using vacuum induction melting and vacuum arc remelting followed by rotary forging and ring rolling. The material was subjected to a standard heat treatment after ring rolling: a solution cycle at 968 °C for 1 hour and oil quench, followed by a two-step aging at 788 °C for 8 hours and at 704 °C hold for 8 hours, then air-cooled. A typical microstructure of the as-received 718Plus superalloy is shown in Figure 1. The microstructure consists of  $\gamma$  matrix grains of an average size of 54  $\mu\text{m}$  with uniformly distributed  $\gamma'$  precipitates within grain interiors (Figure 1b, inset) and plate-like  $\eta$  and  $\delta$  phases (or their combinations<sup>[13]</sup>) at the grain boundaries. The average diameter of  $\gamma'$  precipitates is 27.5 nm. The volume fraction of  $\gamma'$  phase is 16.8 pct, while the volume fraction of  $\eta/\delta$  platelets is 4.4 pct. Furthermore, a small amount of M(C, N) carbonitrides (where M = Nb, Ti) is randomly distributed within the 718Plus microstructure and represents up to 1 pct of its phase composition. The quantitative results were obtained from micrographs. Microhardness in the as-received, fully heat-treated condition was 454 HV<sub>10</sub>.

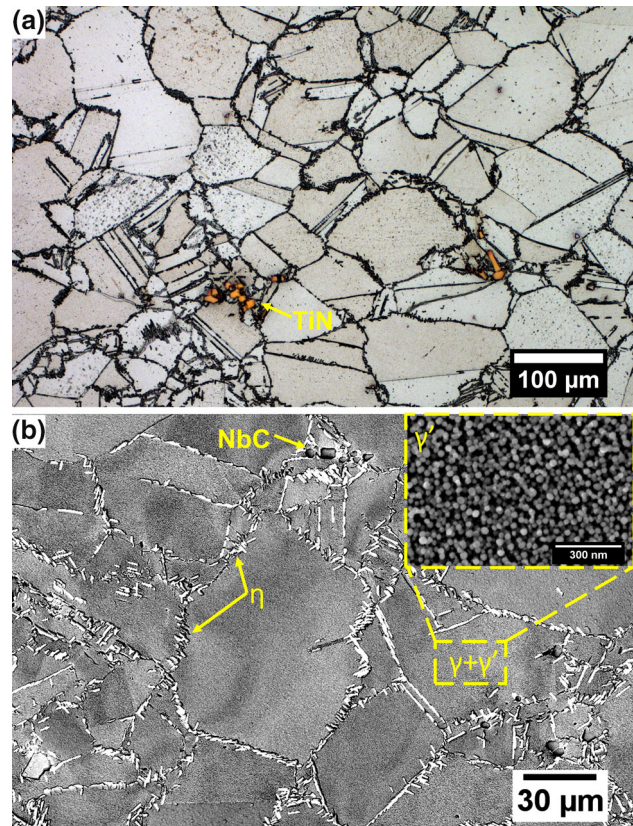


Fig. 1—Typical image of the as-received 718Plus microstructure: (a) LM, Kalling's etch. Gold particles are titanium nitrides, and (b) SEM-SE, inverted contrast. White plate-like precipitates at grain boundaries are  $\eta$  phase, blocky particles are NbC carbides. The inset presents  $\gamma'$  precipitates within  $\gamma$  matrix grains.

### B. Heat Treatment with a Temperature Gradient

Heat treatment with a temperature gradient was performed in an in-house built box furnace with a  $75 \times 75 \times 150$  mm hot zone. The heating elements were reconfigured to obtain a temperature gradient. Additionally, a  $50 \times 50$  mm hole was cut in the middle of the door to allow the heat near the front to escape. A schematic drawing of the furnace is present in Figure 2(a). A rectangular bar with a  $20 \times 20$  mm cross-section and 100 mm length was cut from the ring and instrumented with TCs to record the temperature gradient along the bar. Eight 1.6 mm in diameter and 10-mm deep holes were drilled along the centerline of the bar to hold the TCs, as shown in Figure 2(b). The bar was subjected to a 1-hour gradient heat treatment around the solution temperature, ranging between  $907^\circ\text{C}$  and  $1095^\circ\text{C}$ , followed by a water quench. The solution treatment parameters were based on the standard heat treatment, so the time was fixed as 1 hour. The graded solution temperature range was based on TTT diagram developed by Xie *et al.*<sup>[22]</sup> The temperature range was selected to include main phase transformations present in the diagram and allowed to investigate the influence of different phases on the mechanical properties of 718Plus superalloy. The measured temperatures at TCs locations from the back wall of the furnace to the front door were as follows:  $1093^\circ\text{C}$ ,  $1088^\circ\text{C}$ ,  $1077^\circ\text{C}$ ,  $1061^\circ\text{C}$ ,  $1040^\circ\text{C}$ ,  $1002^\circ\text{C}$ ,  $954^\circ\text{C}$ , and  $907^\circ\text{C}$ . All temperatures did stabilize after 15 minutes of heating.

### C. Thermodynamic Simulations

To compare the phase stability limits of 718Plus after graded treatment with phase stability at equilibrium conditions, Thermo-Calc (version 2020b) software<sup>[31]</sup> (Thermo-Calc Software AB, Solna, Sweden) was utilized. For thermodynamic calculations, a TCNI10 database for Ni-alloys was used. The input chemical composition of 718Plus is given in Section II-A.

### D. Sample Preparation and Material Characterization Methods

In the present study, light microscopy (LM), scanning- and transmission electron microscopy (SEM and TEM) were employed to perform microstructural characterization.

To acquire LM images, AXIO Imager (Zeiss, Oberkochen, Germany) microscope was used. The SEM images were obtained using a high-resolution Merlin Gemini II (Zeiss, Oberkochen, Germany) microscope equipped with a Schottky field emission gun. For imaging on-axis, an in-lens secondary electron (SE) detector was used to minimize the shadowing effect. The samples for LM and SEM were cut from bars at a location in the vicinity of TCs' holes using a low-speed diamond saw. They were mounted in a conducting resin, mechanically ground, and polished using acidic alumina and colloidal silica suspensions. For chemical etching Kalling's reagent was used. Electrochemical etching was performed in 10 pct solution of oxalic acid in distilled water utilizing 3 V electric potential.

TEM analyses were performed using a Tecnai G2 20 TWIN (ThermoFisher, Eindhoven, Netherlands) microscope equipped with a  $\text{LaB}_6$  cathode. Investigations included bright- and dark-field imaging (BF, DF, respectively) and selected area electron diffraction (SAED). Thin foils for TEM examination were cut using a low-speed diamond saw and ground to a thickness below  $40\ \mu\text{m}$ . The final step utilized twin-jet electropolishing with the Tenupol5 (Struers, Ballerup, Denmark) apparatus using 10 pct perchloric acid in a glacial acetic acid electrolyte at temperature 283 K and 50 V electric potential.

Microhardness testing was performed utilizing TUKON 2500 apparatus (Buehler, Esslingen, Germany) using a 98.07 N load and the holding time of 10 seconds. Microhardness measurements were performed along the temperature gradient with a 2 mm spacing between each measure. Each value of microhardness is an average of three measurements.

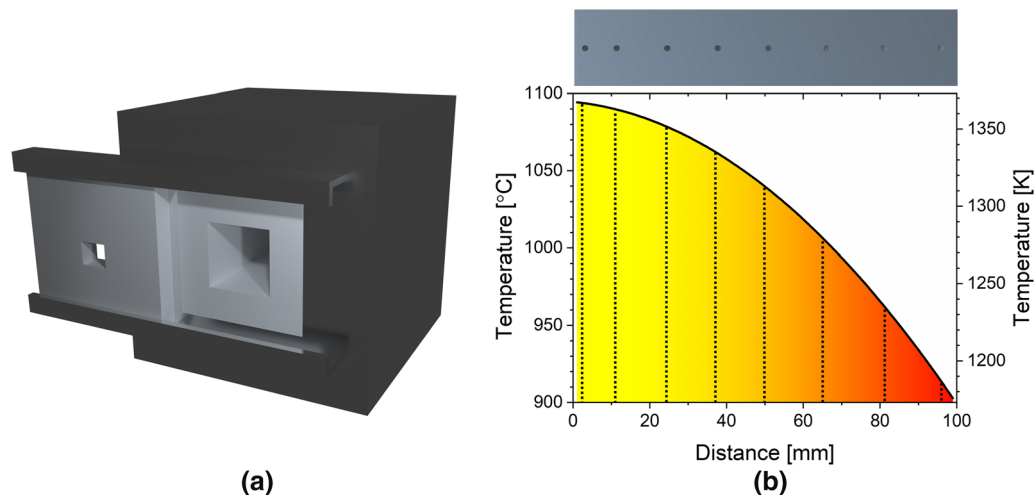


Fig. 2—(a) Drawing of the furnace used for graded heat treatment, and (b) the solution temperature gradient in a function of the sample distance. Dotted lines indicate the location of each thermocouple (TC), which were placed in holes drilled along the tested bar.

### E. Image Analysis

The image analysis was performed on SEM images for grain size,  $\gamma'$  phase, and  $\eta$  phase. The volume fraction of primary carbides was determined based on LM images. To ensure the data reliability, the images for analyses were acquired vertically above the holes drilled for TCs. The image analyses were performed using Fiji (ImageJ) software.<sup>[32]</sup> Standard image analysis procedures were applied when necessary, including image scaling, brightness/contrast enhancement, thresholding, and binarization. To obtain quantitative information about phases, we adopted the Cavalieri–Hacquet principle, where

$$V_V = A_A = L_L. \quad [1]$$

which means that the fraction of each phase in the investigated volume ( $V_V$ ), area ( $A_A$ ), and length ( $L_L$ ) is the same. Originally, this principle was used for LM images, where a single plane of material is observed. To minimize the interaction volume in SEM, *i.e.*, make it comparable to a single plane, we used a low accelerating voltage of 3 to 5 kV and a current of 100 to 120 pA for imaging in SEM-SE. Furthermore, obtained results were supported by quantifying precipitates using 3D tomographic methods, as demonstrated in a previous study.<sup>[33]</sup>

Grain size analyses were performed on a sample size of 100 grains. The analyses were performed on SEM-SE images of non-etched 718Plus superalloy acquired at an accelerating voltage of 5 kV. To minimize the effect of pixel size on the analyses, the images were acquired at a resolution of  $2048 \times 1536$  pixels and a dwell time of at least 40 seconds. Twin boundaries were ignored during the grain size evaluation.

The volume fraction of  $\eta$  phase was analyzed on SEM-SE images of 718Plus superalloy etched with 10 pct solution of oxalic acid in distilled water. It was measured from at least three images that were binarized. Images were acquired at an accelerating voltage of 5 kV.

The volume fraction of carbides was determined on the basis of binarized LM images.

Quantitative analysis of  $\gamma'$  precipitates (as-received material) was done on SEM-SE images acquired at low accelerating voltage of 3 to 5 kV and current of 100 to 120 pA. The obtained results were supported and validated by quantification of precipitates using 3D tomographic methods (STEM-EDXS and FIB-SEM), as demonstrated in our previous study.<sup>[34]</sup>

## III. RESULTS

Application of graded solution treatment resulted in the graded microstructure of 718Plus superalloy along the whole bar. To make it easier for the reader to follow the results, microstructure at TC locations will be presented for general comparison.

### A. Microstructure

Figure 3 shows low-magnification LM images of 718Plus superalloy microstructure after 1-hour graded

solution at the TC locations. The temperature difference between the first four TCs was roughly 30 °C, so changes in grain size at these locations were negligible (see also Table I). The further from the furnace's back wall, the greater was the temperature slope (Figure 2), coupled with more noticeable changes in grain size. The primary role of the  $\eta$  phase in 718Plus superalloy is grain boundary pinning to inhibit grain growth during processing and solution treatment. Based on the most pronounced change in the grain size, shown in Figure 3, it was determined that the solvus temperature of the  $\eta$  phase lies somewhere between the temperature of 1002 °C and 1040 °C. Thus, the microstructure in the vicinity of the TC6 (1002 °C) was investigated in detail.

Figure 4 shows an enhanced resolution LM image of the 718Plus microstructure after 1-hour solution treatment near the temperature of 1002 °C. The resolution of the image was enhanced by the acquisition of series of images at higher magnification and stitching them using the Zeiss MosaiX module. The microstructure on the far-left side of the image was exposed to a solution temperature of about 1008 °C, while the microstructure on the far-right side to a temperature of about 993 °C. At first glance, there is no noticeable change in the microstructure; however, examination of the highlighted areas at higher magnifications revealed clear differences. The microstructure on the right side of Figure 4, exposed to a temperature of about 993 °C, exhibits a bimodal distribution of grains. On the contrary, the grain size on the left side, where the material was exposed to about 1008 °C, is more uniform. These grain size differences are due to the dissolution of the  $\eta$  phase, and in consequence, unpinning of the  $\gamma$  grains. At the TC location, equiaxial grains are present, although a trace amount of  $\eta$  phase is still present, mainly at twin boundaries.

The grain size (diameter) at each TC location was determined based on measurements taken from both LM and SEM images and is summarized in Table I. For temperatures below 1000 °C, where clusters of small grains were present, only larger grains were used for calculation. The grain size at the highest temperature of 1093 °C was 227.1  $\mu\text{m}$ , while at the lowest temperature of 907 °C, 63.5  $\mu\text{m}$ . Generally, the grain size can be divided into two groups, above the  $\eta$  solvus temperature (TC1–5) and below this temperature (TC6–8). Grains below  $\eta$  solvus temperature had a mean diameter below 100  $\mu\text{m}$ , while these above  $\eta$  solvus had a mean diameter above 100  $\mu\text{m}$ . Despite grain size pinning by  $\eta$  phase, slight grain growth was observed even at the lowest temperature of 907 °C, where the grains were larger than in 718Plus superalloys in the as-received condition (54.3  $\mu\text{m}$ ).

Figure 5 shows SEM-SE images highlighting the most significant microstructural changes in 718Plus microstructure upon applied graded solution treatment. The selected images present the microstructure at four thermal states: slightly below (950 °C) and above (970 °C) the  $\gamma'$  phase solvus temperature, slightly above the  $\eta$  phase solvus temperature (1020 °C), and at the highest solution treatment temperature (1095 °C). Changes in size and volume fraction of  $\gamma'$  precipitates

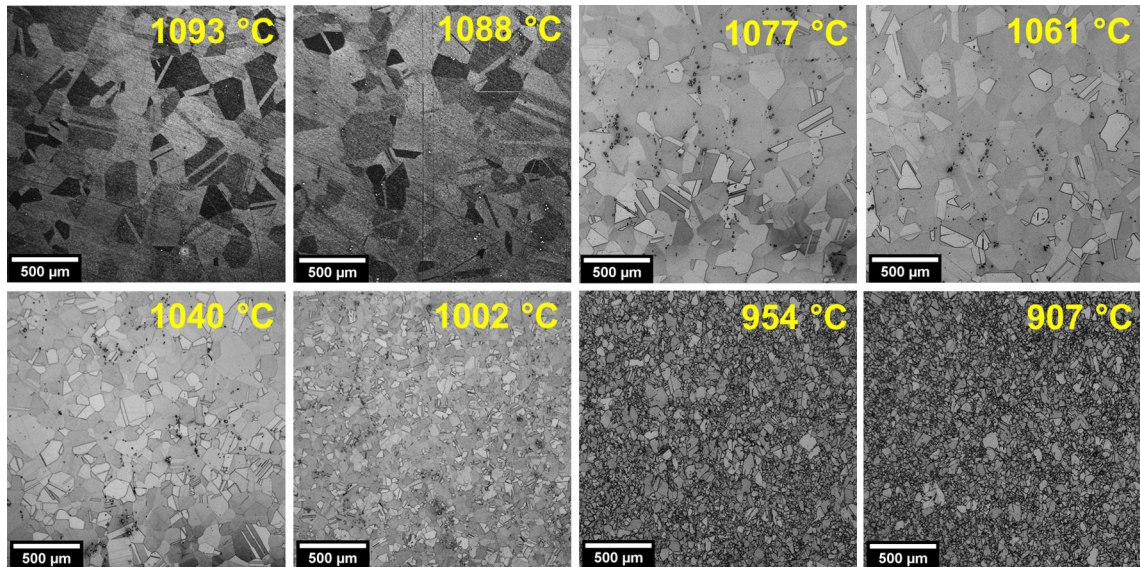


Fig. 3—LM images of 718Plus superalloy microstructure after 1-hour solution treatment with graded temperature. Images were acquired at thermocouples location; the measured temperature is indicated in each image.

**Table I. Grain Size at Thermocouple Location of 718Plus Superalloy Subjected to 1-Hour Graded Solution Treatment**

Thermocouple	TC1	TC2	TC3	TC4	TC5	TC6	TC7	TC8
Measured Temperature (°C)	1093	1088	1077	1061	1040	1002	954	907
Grain Size Diameter (μm)	227.1 ± 66.5	226.4 ± 63.6	217.3 ± 57.2	207.9 ± 61.1	161.8 ± 34.4	85.3 ± 21.9	75 ± 28.3	63.5 ± 21.2

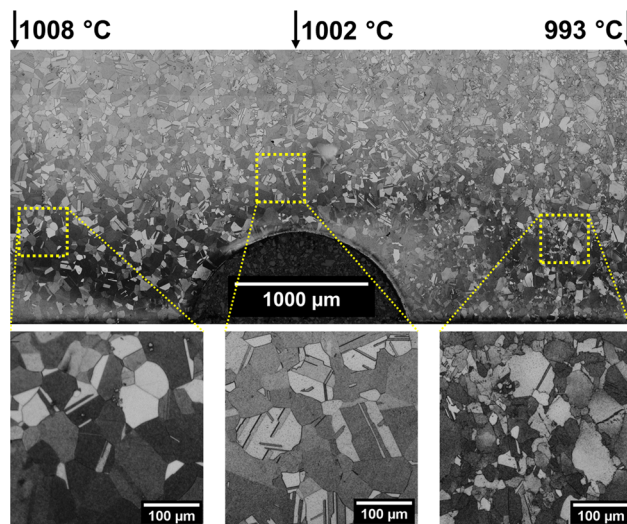


Fig. 4—LM image of the 718Plus microstructure after 1-hour solution treatment neat temperature of 1002 °C. Half-circle at the bottom corresponds to the hole for thermocouple.

can be noted. In the as-received conditions,  $\gamma'$  mean diameter was 27.5 nm, while at the highest temperature before the dissolution, its size exceeded 100 nm. Prior to the graded solution treatment, the  $\eta$  phase was

predominantly present at the grain boundaries, while with an increase of the solution temperature, a decreasing amount of  $\eta$  precipitates was observed. Furthermore, change in the appearance of the  $\eta$  phase was observed, from the continuous platelets at grain boundaries to their random presence as a single  $\eta$  platelet and finally absence at higher temperatures, above 1000 °C.

Based on the results of the microstructural investigation, three ranges of phase stability were established. The least stable among three investigated phases ( $\gamma$ ,  $\gamma'$ ,  $\eta$  phases) was  $\gamma'$  phase with solvus temperature at about 960 °C. The solvus temperature of the  $\gamma'$  phase was further confirmed by TEM, through a detailed examination of a sample solution treated at 970 °C (Figure 6). It may be seen that after 1-hour solution treatment at 970 °C, the  $\gamma$  grains were free from the  $\gamma'$  precipitates. This observation was confirmed by SAED, where the diffraction pattern solved for the  $\gamma$  phase in a [001] zone axis (Figure 6, inset) lacks characteristic spots from the  $\gamma'$  superlattice.

The exact solvus temperature of the  $\eta$  phase was difficult to determine due to its inhomogeneity and predominant presence at the grain boundaries in the microstructure of the 718Plus superalloy. Therefore, the change of  $\eta$  platelets from continuous to the single randomly deployed platelets was chosen as a determining parameter. Figure 7 shows SEM-SE images of  $\eta$

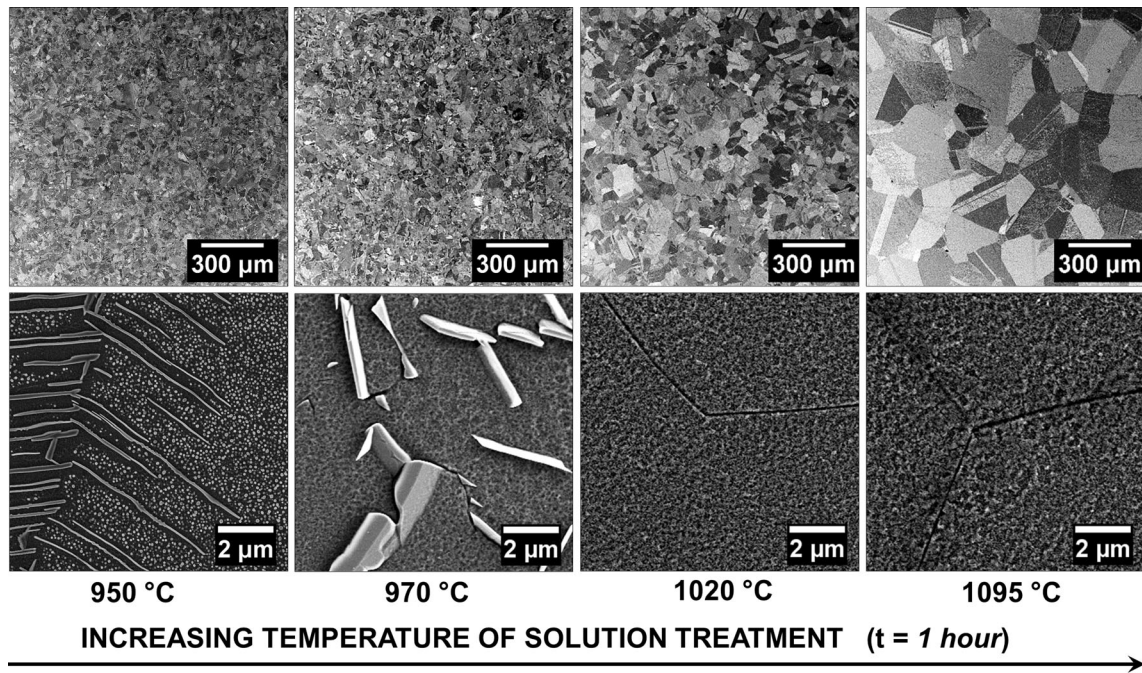


Fig. 5—SEM-SE images highlighting major microstructural differences in 718Plus superalloy after 1-hour graded solution treatment. Samples were electrochemically etched.

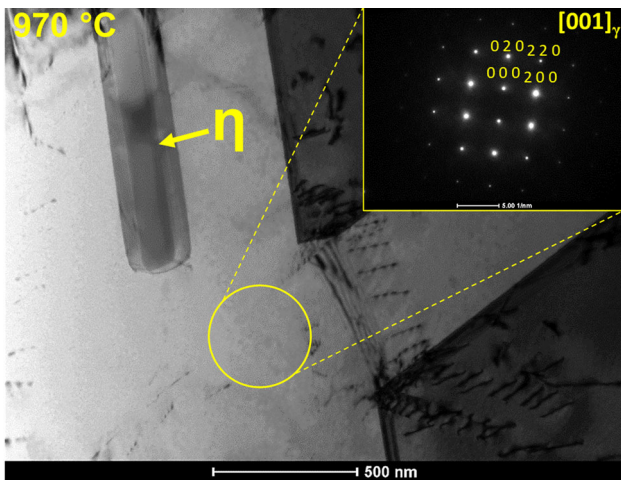


Fig. 6—TEM-BF image of 718Plus superalloy microstructure after 1-hour solution treatment at 970 °C. The microstructure is free from  $\gamma'$  precipitates as confirmed by SAED pattern (inset), solved for the  $\gamma$  phase in [001] zone axis.

phase dissolution within the narrow range of 985 °C to 1002 °C. The image at 1002 °C was acquired at TC6 location, while the following images were acquired with a 1 mm step toward TC7. The temperatures were estimated based on the slope of the gradient solution treatment curve. The volume fraction of  $\eta$  phase in 718Plus superalloy in the as-received condition was calculated as 4.4 pct. Here, the volume fraction changed from roughly 3.8 pct at a temperature of 985 °C to 0.13 pct at 999 °C or single plate at 1002 °C. Based on the

microstructural study, the  $\eta$  phase solvus temperature was established at 1005 °C.

### B. Mechanical Properties

The mechanical properties of 718Plus superalloy after 1-hour solution treatment with graded temperature were investigated using Vickers hardness test. The hardness measurements in the function of solution treatment temperature are shown in Figure 8.

As previously mentioned, three ranges of phase stability were established *via* microscopic observations, and those ranges remarkably correspond with hardness measurement, as indicated by red dashed lines. At the lowest “solution” temperature of 907 °C, the hardness was 325 HV<sub>10</sub>, roughly 30 pct lower than in fully heat-treated conditions. This is related to coarsening of  $\gamma'$  precipitates coupled with decreasing of their volume fraction. The hardness decrease was observed down to the complete dissolution of the  $\gamma'$  phase at 960 °C. Within the range of  $\gamma + \eta$  phases stability, the second decrease of hardness is observed, namely from 270 HV<sub>10</sub> at 960 °C down to 250 HV<sub>10</sub> at 1002 °C. This is related to the decreasing volume fraction of the  $\eta$  phase (see Figure 7), followed by the complete dissolution of this phase.

Interestingly, complete dissolution of the  $\eta$  phase was followed by a significant drop in hardness, which was not observed for the complete dissolution of the  $\gamma'$  phase. Within the  $\gamma$  phase range, the hardness varies between 180 and 200 HV<sub>10</sub> with an average of 192 HV<sub>10</sub>. The hardness remains stable, despite the growth of the  $\gamma$  grains from 85.3  $\mu\text{m}$  at 1002 °C to 227.1  $\mu\text{m}$  at 1093 °C.

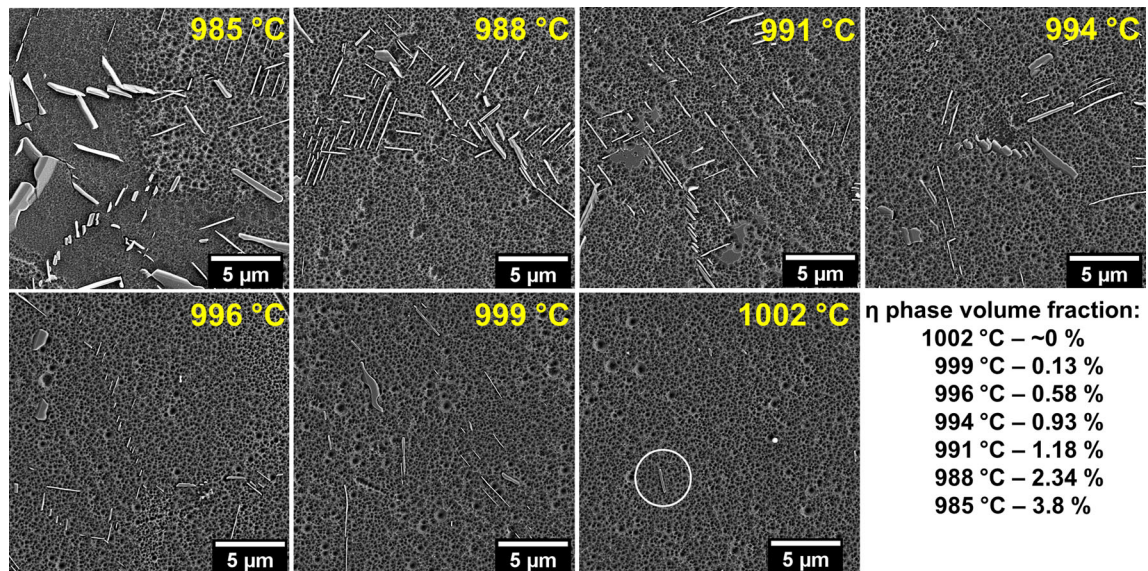


Fig. 7—SEM-SE images highlighting the change of  $\eta$  phase volume fraction in 718Plus superalloy at different temperatures after 1-hour graded solution treatment.

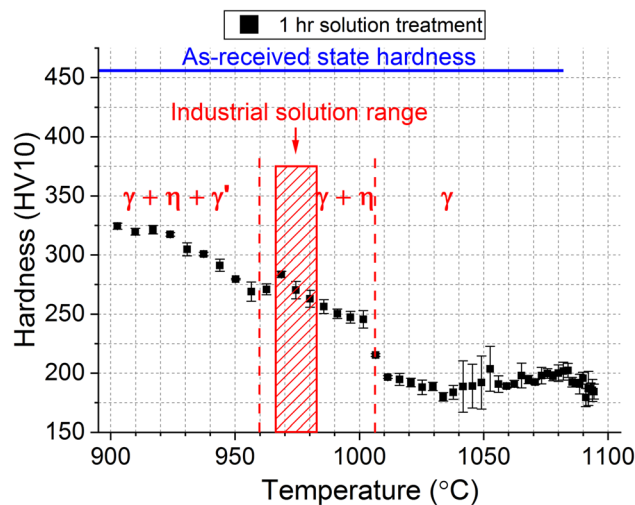


Fig. 8—Change of hardness ( $HV_{10}$ ) in a function of 1-hour graded solution treatment temperature. Error bars represent the standard deviation of hardness measurements (Color figure online).

### C. Thermodynamic Calculations

Thermodynamic calculations of 718Plus phase composition at equilibrium conditions were computed for comparison with experimental results. Figure 9 shows the calculated phase composition of 718Plus superalloy between 500 °C and 1500 °C. In 718Plus superalloy, the formation of two types of carbides is possible, primary MC-type carbides and  $M_{23}C_6$  carbides. Primary MC-type carbides precipitate from the liquid phase and are stable at a high-temperature range, from 650 °C to 1280 °C. In the present study, they were present at all investigated temperatures in the form of Ti- and Nb-rich carbonitrides. However, 1-hour graded solution treatment did not affect them, so they were not evaluated. The  $M_{23}C_6$  carbides were not found at any point in the study. The formation of two types of topologically

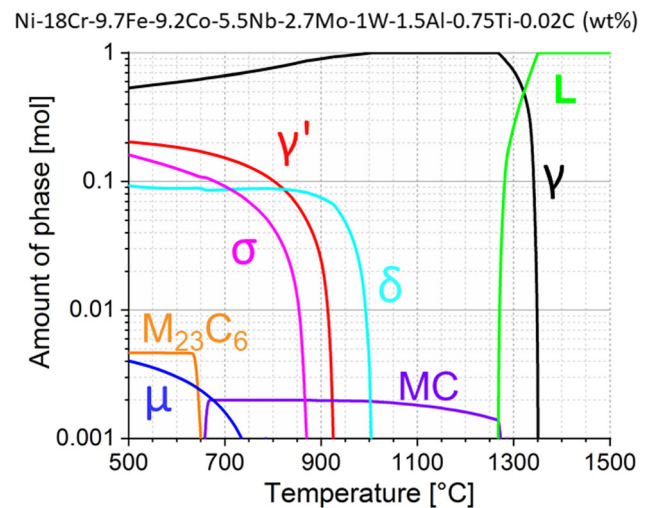


Fig. 9—The calculated equilibrium fraction of phases as a function of temperature in 718Plus superalloy.

close-packed phases ( $\sigma$  and  $\mu$ ) was calculated; however, these types of phases are usually present after long-term thermal exposure.<sup>[15]</sup> So, unsurprisingly they were not observed within this study.

As expected, the  $\gamma$  matrix phase is the most stable phase, up to the liquidus temperature, while the  $\gamma'$  phase is stable up to 925 °C. The maximum volume fraction of the  $\gamma'$  phase calculated at 500 °C was close to 20 vol pct. Under the applied version of the database, the  $\eta$  phase should not be present in 718Plus superalloy; instead, up to 9 vol pct of  $\delta$  phase should be present. It should be stable up to 1005 °C. It is important to note a narrow window of 77 °C between the solvus temperatures of  $\gamma'$  (925 °C) and  $\delta$  (1002 °C) phases. The standard solution step is conducted within this window, between 954 °C and 982 °C. Thus, it is crucial to tightly control the process within this window to avoid the

unnecessary precipitation of  $\gamma'$  phase (below) or dissolution of  $\delta/\eta$  (above), respectively.

## IV. DISCUSSION

### A. Application of Solution Treatment with Temperature Gradient

Application of temperature gradient for 1-hour solution treatment of 718Plus superalloy was successful and resulted in the graded microstructure. This is an original approach to study phase stability in nickel-based superalloys. Over the years, thermoanalytical techniques such as differential scanning calorimetry or dilatometry were used to determine the phase stability limits of alloys. Our approach provides information about phase stability limits supported by full microstructural details, which is unattainable for the abovementioned techniques. In other words, it would require many samples, heating steps, and time to obtain similar microstructural results. In this study, a 1-hour solution treatment within a range of about 200 °C was investigated. This range was chosen to perform the solution treatment in the stability range of three phases— $\gamma$ ,  $\gamma'$ ,  $\eta$  and was based on the TTT diagram showed by Xie *et al.*<sup>[22]</sup> This goal was achieved, and stability limits of  $\gamma'$  and  $\eta$  phases were established based on microstructural changes.

The gradient of mechanical properties in terms of hardness was obtained as well. It was helpful to determine the phase stability limits, as different phases provided different strengthening effects. Based on the hardness measurements in the  $\gamma$  range only, a base value was determined (without precipitation hardening effect) between 180 and 200 HV<sub>10</sub>. Change of grain size within the  $\gamma$  phase range (above 1005 °C) suggests that grain size does not affect the hardness within the investigated range in a meaningful manner. However, this parameter alone is not enough to determine other mechanical properties desired for polycrystalline nickel-based superalloys, like creep resistance or low cycle fatigue behavior. Nevertheless, selected variants of heat treatment may be selected for further examinations.

Recently, a similar approach employing samples exposed to thermal gradient was used by Wei and Zhao,<sup>[35]</sup> who investigated Fe–Cr–Mo ferritic steel. They achieved a temperature gradient of 400 °C on a 4.5-in. bar, used for 10-hour aging treatment. The microstructural gradient can be obtained using arc methods<sup>[36]</sup> or with a water circulation system.<sup>[37]</sup> Nevertheless, for the fundamental study of phase stability and quantitative analyses, more narrow temperature gradients should be desired, as demonstrated within the present study.

### B. Phase Stability Limits

The main objective of graded solution treatment was to determine the phase stability limits in the 718Plus superalloy. This goal was achieved by both microstructural and hardness studies. The solvus temperature of  $\gamma'$  phase was defined as 960 °C, while  $\eta$  phase solvus was 1005 °C. Thermodynamic calculations of phase

composition at equilibrium conditions were used for comparison with the experimental results (Figure 9).

When it comes to the main investigated phases  $\gamma'$  and  $\delta/\eta$ , the calculated results were in partial agreement with the experimental ones. The calculated solvus temperature of the  $\gamma'$  phase at 925 °C is about 35 °C lower than the microstructural changes observed during graded solution treatment. This may be important from the processing point of view. For  $\delta/\eta$  phases, the biggest downside is the prediction of  $\delta$  phase instead of  $\eta$  phase. The information about the presence of the  $\delta$  phase may be found in many early works,<sup>[8,11,38]</sup> however, later data unambiguously confirm dominant presence of the  $\eta$  phase in 718Plus superalloy.<sup>[12,13,15,33]</sup> Nevertheless, with the assumption that the calculated temperature stability of  $\delta$  phase is, in fact, the stability of  $\eta$  phase, the calculated temperature of 1002 °C is in good agreement with that observed *via* microstructural changes in solution-treated sample (about 1005 °C). Comparable results were obtained by Löhnert and Pyczak,<sup>[39]</sup> who investigated phase stability using JMatPro software with the TTNi7 database. They calculated the solvus temperature of the  $\gamma'$  phase at 976 °C and the  $\delta$  phase at 1026 °C, which are a bit higher values, but still close to those within the present study. Furthermore, both values are lower than the early modeling results obtained by Cao,<sup>[40]</sup> who calculated the solvus of the  $\delta$  phase at 1065 °C and  $\gamma'$  phase at 995 °C using JMatPro software. Other authors<sup>[12,14]</sup> reported attempts to predict the volume fraction of  $\eta$  phase in 718Plus superalloy. However, to force the prediction of the  $\eta$  phase, it is necessary to suppress the  $\delta$ ,  $\gamma'$ , and  $\gamma''$  phases from the computation.

The input data are the most critical factor affecting the results of the equilibrium phase stability calculations. Even slight variations in chemical composition may influence the output results. For instance, Löhnert and Pyczak<sup>[37]</sup> used a smaller amount of iron to calculate the phase stability of 718Plus superalloy (9 vs 9.7 wt pct in the present study). Furthermore, ongoing improvement of databases and models influences the results as well.

Early studies on phase stability in 718Plus superalloy were performed by Xie *et al.*<sup>[11,22]</sup> The authors combined conventional heat treatment with hardness tests and structural analyses to construct a TTT diagram for the 718Plus superalloy. They determined solvus temperature of the  $\gamma'$  phase at 989 °C and the  $\delta$  phase at 1060 °C. In comparison to the present results, both values were overestimated. This highlights added importance provided by graded heat treatment, where those ranges can be precisely determined. Later, Cao<sup>[40]</sup> measured the solvus temperature of the  $\gamma'$  phase by differential thermal analysis as 963 °C, which is in line with the present study. It was concluded that  $\delta$  phase solvus is between 1002 °C and 1018 °C, measured using metallographic methods. Another thermoanalytical research was conducted by Casanova *et al.*,<sup>[14]</sup> who used differential scanning calorimetry. They measure the solvus of the  $\gamma'$  phase as 967 °C while  $\delta/\eta$  phases as 1012 °C. The starting temperatures for dissolution were 963 °C and 998 °C for  $\gamma'$  and  $\delta/\eta$  phases, respectively.



As previously mentioned, M(C, N)-type carbides/nitrides were stable at the investigated range. The measured volume fraction of these precipitates in the solution-treated samples varied between 0.25 and 0.39 pct at the TC positions. In 718Plus superalloy, the M(C, N) precipitates are randomly distributed within the microstructure (if not significantly affected by the processing technology, *i.e.*, rolling), and they do not provide any specific strengthening effect, like grain boundary strengthening. Therefore, the change in their fraction (without any particular trend) did not affect the hardness.

The values determined within the present work were in good agreement with most of the data obtained by thermoanalytical methods.

### C. Strengthening Effect of the $\eta$ Phase

For 1-hour solution treatment, a two-phase range was established between 960 °C and 1005 °C, where only  $\gamma$  and  $\eta$  phases were present (Figure 8). Within this range, decrease in hardness was observed along with the reduction of  $\eta$  phase volume fraction. The volume fraction of the  $\eta$  phase decreased with increasing solution treatment temperature. Within the two-phase range, the highest hardness of 285 HV<sub>10</sub> was measured for solution treatment at 968 °C, while above that temperature, a continuous decrease of hardness down to 250 HV<sub>10</sub> at 1000 °C was observed. As mentioned previously, the base hardness of the  $\gamma$  phase ranged from 180 to 200 HV<sub>10</sub>. Thus, by subtracting the hardness of the  $\gamma$  phase, it is possible to approximate the strengthening effect of the  $\eta$  phase. Assuming that the base hardness of  $\gamma$  phase solid solution is equal to 190 HV<sub>10</sub>, the increase of hardness resulting from the introduction of  $\eta$  phase at 1000 °C is 60 HV<sub>10</sub> or roughly 30 pct (Figure 8). At solution temperature of 968 °C, the volume fraction of the  $\eta$  phase should be like in the as-received material, so 4.4 pct. At this temperature, the hardness increase was measured as 95 HV<sub>10</sub> or about 50 pct compared to the base hardness of  $\gamma$  phase solid solution.

Several authors described strengthening effects in polycrystalline nickel-based superalloys,<sup>[41–49]</sup> where unimodal as well as multimodal strengthening mechanisms were considered. Roth *et al.*<sup>[45]</sup> and Ritter *et al.*<sup>[49]</sup> focused their works on solid-solution strengthening. The first study focused on predicting yield strength, while the second only focused on the influence of particular elements on transition temperatures. Kozar *et al.*<sup>[41]</sup> study was one of the first that considered multimodal strengthening in P/M polycrystalline nickel-based superalloy, IN100. Their calculations account for solid-solution strengthening, Hall–Petch effect, precipitates shearing, dislocation bowing, and precipitates size distribution. Kozar *et al.*<sup>[41]</sup> and later Goodfellow<sup>[48]</sup> pointed out that many of the strengthening mechanisms crossover, creating further difficulties during calculation. Later, Goodfellow *et al.*<sup>[46]</sup> calculated yield strength for six commercial superalloys using strengthening by precipitation of  $\gamma'$  phase, solid solution, coherency, grain boundaries, and Orowan mechanism. Notably, recalled articles and recent reviews<sup>[43,48]</sup> do not consider the strengthening effect of grain boundary precipitates neither in the form of  $\delta$  phase present in IN718

superalloy nor  $\eta$  phase 718Plus superalloy. The present study does not fulfill this gap perfectly; however, the strengthening effect of the  $\eta$  phase was extracted to some extent. In the future, these data may be used to create a model, which will incorporate this strengthening mode.

In the end, it is necessary to underline that occurring grain growth of the  $\gamma$  grains is not limited only to the dissolution of the  $\eta$  phase. In alloys, recrystallization occurs at high temperatures. Sommitsch *et al.*<sup>[50]</sup> investigated 718Plus superalloy in terms of dynamic and static recrystallization. They have found that after isothermal annealing for 6 hours at 1000 °C, the fraction of recrystallized grains was only 7 pct. Moreover, they did not observe any grain growth below the temperature of 975 °C. These observations support the significant role of the  $\eta$  phase in pinning the grain boundaries.

## V. CONCLUSIONS

The 718Plus superalloy was subjected to a solution treatment examination. A 1-hour solution treatment with graded temperature was applied, where the solution temperature ranged between 907 °C and 1095 °C. The major conclusions of this study are as follows:

- The application of heat treatment with graded temperature successfully resulted in the gradient of microstructure and mechanical properties. This approach may be used to precise design heat treatment protocols cost-effectively.
- The grains size (diameter) of the  $\gamma$  phase changed from 54.3  $\mu\text{m}$  after standard heat treatment, through 63.5  $\mu\text{m}$  at 907 °C up to 227.1  $\mu\text{m}$  at 1095 °C. The grain growth was mainly observed above 1000 °C. This was attributed mainly to dissolution of the  $\eta$  phase that pinned the grains.
- The phase stability was assessed by microstructural investigation. The least stable of the three phases ( $\gamma$ ,  $\gamma'$ ,  $\eta$ ) was the  $\gamma'$  phase with solvus temperature at about 960 °C, which was confirmed by electron diffraction. The solvus temperature of the  $\eta$  phase was determined based on the decreasing volume fraction of plate-like precipitates and was established at 1005 °C.
- The structure–property relationship between 718Plus superalloy microstructure and mechanical properties was established. The change of the  $\gamma$  phase grain size in the single-phase range did not affect the hardness in a meaningful manner. Significant increases in hardness were observed after the introduction of  $\gamma'$  and  $\eta$  phases.

## ACKNOWLEDGMENTS

The authors acknowledge Pratt & Whitney, CT, for providing the material used in this investigation and performing heat treatments, as well as for financial support under Contract No 24117. A part of the study was conducted within fundamental research financed by

AGH University of Science and Technology under Project Number 16.16.110.663. K.W. was supported by the EMPAPOSTDOCS-II Program that has received funding from the European Union's Horizon 2020 Research and Innovation Program under the Marie Skłodowska-Curie Grant Agreement Number 754364.

## DATA AVAILABILITY

The raw/processed data required to reproduce these findings cannot be shared at this time as the data form part of an ongoing study.

## CONFLICT OF INTEREST

On behalf of all authors, the corresponding author states that there is no conflict of interest.

## OPEN ACCESS

This article is licensed under a Creative Commons Attribution 4.0 International License, which permits use, sharing, adaptation, distribution and reproduction in any medium or format, as long as you give appropriate credit to the original author(s) and the source, provide a link to the Creative Commons licence, and indicate if changes were made. The images or other third party material in this article are included in the article's Creative Commons licence, unless indicated otherwise in a credit line to the material. If material is not included in the article's Creative Commons licence and your intended use is not permitted by statutory regulation or exceeds the permitted use, you will need to obtain permission directly from the copyright holder. To view a copy of this licence, visit <http://creativecommons.org/licenses/by/4.0/>.

## REFERENCES

1. S. Patel, J. Debarbadillo, and S. Coryell: in *Superalloy 718 and Derivatives*, vol. 1, Springer, 2018, pp. 23–49.
2. K. Kulawik, P.A. Buffat, A. Kruk, A.M. Wusatowska-Sarnek, and A. Czyska-Filemonowicz: *Mater. Charact.*, 2015, vol. 100, pp. 74–80.
3. J.F. Radavich: in *Superalloys 718 Metallurgy and Applications*, vol. 1, 1989, pp. 229–40.
4. J.M. Oblak, D.F. Paulonis, and D.S. Duvall: *Metall. Trans.*, 1974, vol. 5, pp. 143–53.
5. R. Cozar and A. Pineau: *Metall. Trans.*, 1973, vol. 4, pp. 47–59.
6. A. Oradei-Basile and J.F. Radavich: in *Superalloys 718, 625 and Various Derivatives*, 1991, pp. 325–35.
7. R.E. Schafrik, D.D. Ward, and J.R. Groh: in *Superalloys 718, 625, 706 and Various Derivatives*, 2001, pp. 1–11.
8. R.L. Kennedy: in *Superalloys 718, 625, 706 and Various Derivatives 2005*, 2005, pp. 1–14.
9. E.A. Ott, J. Groh, and H. Sizek: in *Superalloy 718, 625, 706 and Derivatives 2005*, 2005, pp. 35–45.
10. W.-D. Cao and R. Kennedy: in *Superalloys 2004*, 2004, pp. 91–99.
11. X. Xie, G. Wang, J. Dong, C. Xu, W.-D. Cao, and R. Kennedy: *Superalloys 718, 625, 706 and Various Derivatives (2005)*, 2005, pp. 179–91.
12. E.J. Pickering, H. Mathur, A. Bhowmik, O.M.D.M. Messé, J.S. Barnard, M.C. Hardy, R. Krakow, K. Loehnert, H.J. Stone, and C.M.F. Rae: *Acta Mater.*, 2012, vol. 60, pp. 2757–69.
13. O.M. Messé, J.S. Barnard, E.J. Pickering, P.A. Midgley, and C.M.F. Rae: *Philos. Mag.*, 2014, vol. 94, pp. 1132–52.
14. A. Casanova, M.C. Hardy, and C.M.F.F. Rae: in *8th International Symposium on Superalloy 718 and Derivatives*, 2014, pp. 573–86.
15. S. Lech, A. Kruk, G. Cempura, A. Gruszczyński, A. Gil, A. Agüero, A.M. Wusatowska-Sarnek, and A. Czyska-Filemonowicz: *J. Mater. Eng. Perform.*, 2020, vol. 29, pp. 1453–59.
16. M. Wang, Q. Deng, J. Du, Z. Tian, and J. Zhu: *Mater. Trans.*, 2015, vol. 56, pp. 635–41.
17. J. Li, R. Ding, Q. Guo, C. Li, Y. Liu, Z. Wang, H. Li, and C. Liu: *Mater. Sci. Eng. A*, 2021, vol. 812, p. 141113.
18. G.A. Zickler, R. Schnitzer, R. Radis, R. Hochfellner, R. Schweins, M. Stockinger, and H. Leitner: *Mater. Sci. Eng. A*, 2009, vol. 523, pp. 295–303.
19. K.A. Unocic and B.A. Pint: in *8th International Symposium on Superalloy 718 and Derivatives*, 2014, pp. 667–77.
20. A. Kruk, S. Lech, A. Gil, G. Cempura, A. Agüero, A.M. Wusatowska-Sarnek, and A. Czyska-Filemonowicz: *Corros. Sci.*, 2020, vol. 169, p. 108634.
21. S. Lech, A. Kruk, A. Gil, G. Cempura, A. Agüero, and A. Czyska-Filemonowicz: *Scripta Mater.*, 2019, vol. 167, pp. 16–20.
22. X. Xie, C. Xu, G. Wang, J. Dong, W.D. Cao, and R. Kennedy: in *Superalloys 718, 625, 706 and Derivatives 2005*, 2005, pp. 193–202.
23. W.D. Cao: in *Superalloys 2008*, 2008, pp. 789–97.
24. J. Zhang, C. Wu, Y. Peng, X. Xia, J. Li, J. Ding, C. Liu, X. Chen, J. Dong, and Y. Liu: *J. Alloys Compd.*, 2020, vol. 835, p. 155195.
25. B. Xie, B. Zhang, H. Yu, H. Yang, Q. Liu, and Y. Ning: *Mater. Sci. Eng. A*, 2020, vol. 784, p. 139334.
26. R. Hayes, E. Thompson, K. Johnson, and A. Aichlmayr: *Mater. Sci. Eng. A*, 2009, vol. 510–511, pp. 256–61.
27. J. Andersson, G.P. Sjöberg, L. Viskari, and M. Chaturvedi: *Mater. Sci. Technol.*, 2012, vol. 28, pp. 733–41.
28. M. Markl, A. Müller, N. Ritter, M. Hofmeister, D. Naujoks, H. Schaar, K. Abrahams, J. Frenzel, A.P.A. Subramanyam, A. Ludwig, J. Pftzing-Micklich, T. Hammerschmidt, R. Drautz, I. Steinbach, R. Rettig, R.F. Singer, and C. Körner: *Metall. Mater. Trans. A*, 2018, vol. 49A, pp. 4134–45.
29. C. Rae: *Mater. Sci. Technol.*, 2009, vol. 25, pp. 479–87.
30. K. Wiecezrak, O. Nowicka, S. Michalski, T.E.J. Edwards, M. Jain, T. Xie, L. Pethö, X. Maeder, and J. Michler: *Mater. Des.*, 2021, vol. 205, p. 109710.
31. J.O. Andersson, T. Helander, L. Höglund, P. Shi, and B. Sundman: *CALPHAD*, 2002, vol. 26, pp. 273–312.
32. J. Schindelin, I. Arganda-Carreras, E. Frise, V. Kaynig, M. Longair, T. Pietzsch, S. Preibisch, C. Rueden, S. Saalfeld, B. Schmid, J.Y. Tinevez, D.J. White, V. Hartenstein, K. Eliceiri, P. Tomancak, and A. Cardona: *Nat. Methods*, 2012, vol. 9, pp. 676–82.
33. A. Kruk, G. Cempura, S. Lech, A.M. Wusatowska-Sarnek, and A. Czyska-Filemonowicz: in *Proceedings of the 9th International Symposium on Superalloy 718 and Derivatives: Energy, Aerospace, and Industrial Applications*, 2018, pp. 1035–50.
34. A. Kruk, G. Cempura, S. Lech, and A. Czyska-Filemonowicz: *Arch. Metall. Mater.*, 2016, vol. 61, pp. 535–41.
35. C. Wei and J.-C. Zhao: *Materialia (Oxf.)*, 2018, vol. 3, pp. 31–40.
36. V.A. Hosseini, L. Karlsson, K. Hurtig, I. Choquet, D. Engelberg, M.J. Roy, and C. Kumara: *Mater. Des.*, 2017, vol. 121, pp. 11–23.
37. Y. Ning, Z. Yao, H. Guo, and M.W. Fu: *J. Alloys Compd.*, 2013, vol. 557, pp. 27–33.
38. P.J. Ennis, A. Strang, S.P. Gill, G.M. McColvin, and H.V. Atkinson: *Energy Mater.*, 2012, vol. 4, p. 4.
39. K. Löhner and F. Pyczak: in *7th International Symposium on Superalloy 718 and Derivatives*, 2010, pp. 877–91.
40. W.D. Cao: in *Superalloys 718, 625, 706 and Various Derivatives 2005*, 2005, pp. 165–77.
41. R.W. Kozar, A. Suzuki, W.W. Milligan, J.J. Schirra, M.F. Savage, and T.M. Pollock: *Metall. Mater. Trans. A*, 2009, vol. 40A, pp. 1588–1603.

42. T.M. Smith, B.D. Esser, N. Antolin, A. Carlsson, R.E.A. Williams, A. Wessman, T. Hanlon, H.L. Fraser, W. Windl, D.W. McComb, and M.J. Mills: *Nat. Commun.*, 2016, vol. 7, pp. 1–7.
43. M.C. Hardy, M. Detrois, E.T. McDevitt, C. Argyrakis, V. Saraf, P.D. Jablonski, J.A. Hawk, R.C. Buckingham, H.S. Kitaguchi, and S. Tin: *Metall. Mater. Trans. A*, 2020, vol. 51A, pp. 2626–50.
44. L. Wu, T. Osada, I. Watanabe, T. Yokokawa, T. Kobayashi, and K. Kawagishi: *Mater. Sci. Eng. A*, 2021, vol. 799, p. 140103.
45. H.A. Roth, C.L. Davis, and R.C. Thomson: *Metall. Mater. Trans. A*, 1997, vol. 28A, pp. 1329–35.
46. A.J. Goodfellow, E.I. Galindo-Nava, C. Schwalbe, and H.J. Stone: *Mater. Des.*, 2019, vol. 173, pp. 1–5.
47. A.J. Goodfellow, E.I. Galindo-Nava, K.A. Christofidou, N.G. Jones, C.D. Boyer, T.L. Martin, P.A.J. Bagot, M.C. Hardy, and H.J. Stone: *Acta Mater.*, 2018, vol. 153, pp. 290–302.
48. A.J. Goodfellow: *Mater. Sci. Technol.*, 2018, vol. 34, pp. 1793–1808.
49. N.C. Ritter, R. Sowa, J.C. Schauer, D. Gruber, T. Goehler, R. Rettig, E. Povoden-Karadeniz, C. Koerner, and R.F. Singer: *Metall. Mater. Trans. A*, 2018, vol. 49A, pp. 3206–16.
50. C. Sommitsch, D. Huber, I.S. Fredrik, S. Mitsche, M. Stockinger, and B. Buchmayr: *Int. J. Mater. Res.*, 2009, vol. 100, pp. 1088–98.

**Publisher's Note** Springer Nature remains neutral with regard to jurisdictional claims in published maps and institutional affiliations.